

**Purdue Physics REU conference**  
**Agenda and Abstracts**  
**August 3, 2023, room PHYS 242**

- 9:00 Georgia Nissen. *Optimizing Thermal Interface Material for the Compact Muon Solenoid Detector.* (Dr. Das)
- 9:25 August Larson. *Detection of Tau3Mu Decays Using Machine Learning in the Compact Muon Solenoid.* (Dr. Liu)
- 9:50 Emma Tintinger. *Macro Pixel Sub-Assembly (MaPSA) Testing for CMS Outer Tracker Upgrade.* (Dr. Liu)
- 10:15 Ben Hughes. *Rubidium-87 Magneto-Optical Trap.* (Dr. Hung)
- 10:35 – 10:45 *Break*
- 10:45 Troy Tsubota. *Quantum sensing of paramagnetic ions with spin defects in hexagonal boron nitride.* (Dr. Li)
- 11:05 Betsy Woodward. *Artificial Photosynthesis.* (Dr. Pushkar)
- 11:30 Mary Davenport. *Acoustic Wave Propagation Through Fracture Networks.* (Dr. Pyrak-Nolte)
- 11:55 James Szalkie. *Integration and Assessment of Imaging Techniques in Applied Optics.* (Dr. Nolte)
- 12:20 – 1:30 *Lunch (on your own)*
- 1:30 Nathan Henry. *Control of Superconducting Qubit Systems via RF Frequency Mixing.* (Dr. Ma)
- 1:55 Julia White. *Designing and Implementing PID Controller to aid in Investigating the Photoassociation of Rb-87 Bose-Einstein Condensates.* (Dr. Chen)
- 2:20 Lauren Bell. *Automation of Time Series Giga-hertz Data Streams from Circuits.* (Dr. Banerjee)
- 2:45 Daniel Hoover. *Resonant Tunneling due to Impurities in the  $\nu=1$  Quantum Hall State.* (Dr. Vayrynen)
- 3:10 *The end*
- 6:00 - *Farewell party/picnic at Sergei Savikhin's house for REU students*  
*Advisors & significant others are welcome, but please reply for count!*  
Address: 2505 McShay Dr., West Lafayette  
Phone: 765-413-5026 (cell)

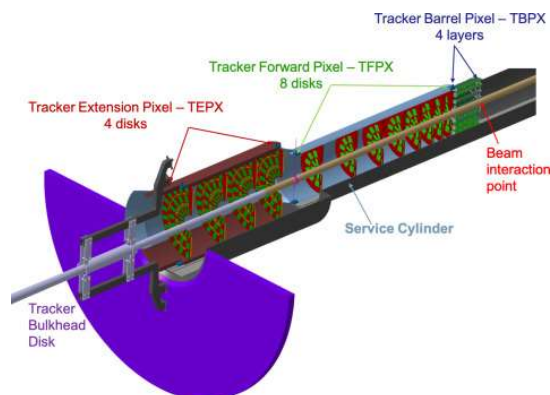
# Optimizing Thermal Interface Material for the Compact Muon Solenoid Detector

Georgia Nissen<sup>1,2</sup>, Souvik Das<sup>2</sup>

<sup>1</sup>Wartburg College, IA, <sup>2</sup>Purdue University, IN

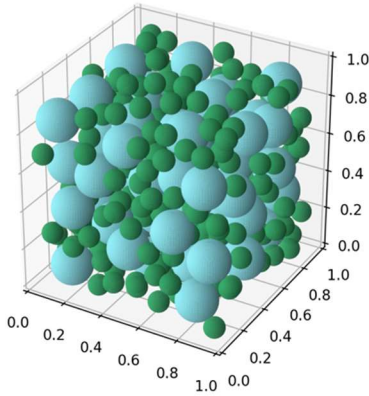
The Large Hadron Collider (LHC) is the world's most powerful particle accelerator located across Switzerland and France. It accelerates protons to reach 13.6 TeV collision energies at four points along the 27 km ring. At one of these collision points lies the Compact Muon Solenoid detector (CMS). This general-purpose detector is used to search for new physics and precisely measure known physics by collecting information about stable particles and analyzing the data. There has been a total of three runs at the LHC with the most recent run ongoing. After this run, the LHC will undergo a High Luminosity (HL-LHC) Upgrade with the goal of producing more collisions to increase the potential of discovering physics beyond the Standard Model.

To take meaningful data in spite of the higher rate of collisions, the CMS detector will undergo Phase II Upgrades that include higher granularities for its Inner Tracker (IT) pixel detector. Higher granularity implies higher power consumption and dissipation, making thermal runaway a serious concern for the IT. This summer, I focused on mitigating thermal runaway in the IT. The IT contains Dee structures, optimized for heat extraction, that hold pixel modules on both sides. These pixels need to be held down with a thermal interface material (TIM). The TIM grease used to hold these pixels in place have a mono-sized distribution of diamond dust mixed in it. Diamond was chosen as the dopant choice as it is



extremely thermally conductive, has a smaller neutron cross section, and is highly radiation resistant.

My goal was to find out if a two-size mixture of diamond particles would increase the



thermal conductivity of the TIM mixture. I did this by first creating a 2-D model of random loose packing with circles. I confirmed density values with visualizations of the code and proceeded to move onto 3-D. Some important aspects that were implemented in the code include a grid structure for randomly placing a new sphere to make it run faster, converting from Python to C++, and creating toroidal

boundaries on both the 2-dimensional and 3-dimensional code. My initial findings found that the density peaks when the small sphere has a size of about 10% than the larger sphere.

This research has pushed me in the direction of finding a phenomenon observed in 3-dimensional random loose packing that is not seen in two dimensions. I will continue this research into the fall to further pursue this phenomenon.

I would like to thank my advisor Souvik Das who has helped me grow tremendously this summer as a student and given me advice and mentorship to help me continue my studies in the coming years. This work was supported by NSF REU grant PHY-2244297.

# Detection of Tau3Mu Decays Using Machine Learning in the Compact Muon Solenoid

August Larson<sup>1,2</sup>, Benjamin Simon<sup>1</sup>, Dr. Miaoyuan Liu<sup>2</sup>

Syracuse University NY, Purdue University IN

High energy physics is a rapidly evolving field based on the Standard Model. Since its conception, attention has been directed to exploring the model's limitations. Beyond Standard Model (BSM) theories such as supersymmetry are prominent extensions proposed to address these limitations. However, confirming these experimentally has proven challenging.

The aim of this project is to research a machine learning model that could search for a tauon to 3 muon decay inside of the Large Hadron Collider's Compact Muon Solenoid (CMS) detector. Finding such a decay could constrain the bounds in which BSM theories exist. This machine learning model would either support or eliminate potential probabilities for BSM extensions based on a calculated probability that a certain number of events that match a tauon to 3 muon will occur in the CMS compared to the number of events actually captured. Two types of machine learning models were examined during this project: a supervised machine learning model (Graph Neural Network - GNN) and an unsupervised machine learning model (Graph Out of Distribution Detection - GoodD). The GNN was fed labeled signal and background datasets, while GoodD was fed only background pileup datasets with the intention that both models would successfully classify background data to be filtered out and signal data which would be stored for analysis.

The specific decay that this project focuses on is a tauon to 3 muon decay and is an example of charged lepton flavor violation. Under the Standard Model, this decay has a branching ratio on the order of  $10^{-55}$ . However, when BSM theories are applied the branching ratio can increase to be on the order of  $10^{-8}$ .

In the Graph Neural Network, edges between nodes have assigned values and weights. These values and weights are multiplied, summed, and then passed through a sigmoid function, compressing the output into a value between 0 and 1. This value identifies the compressed output as either signal (closer to 1) or background (closer to 0) based on a threshold. Additionally, a bias parameter acts as a cutoff, added to the summation prior to the sigmoid curve, excluding values that do not meet the desired threshold. After obtaining the score, the loss function is calculated, indicating how much the final score should be penalized.<sup>1</sup> The negative gradient of this loss function with respect to the learnable parameters points in the direction of the quickest minimization for the loss function. Subsequently, the weights and biases of the GNN are adjusted accordingly, and the entire process is iterated until the loss is minimized as much as possible.<sup>2</sup>

The out-of-distribution detection model, GoodD, follows a different approach. It seeks anomalies deviating from the expected background data by employing multiple perspectives to analyze the dataset. This contrastive learning method aims for reduced variance between datasets, potentially producing a more reliable classifier. GoodD uses perturbation-free data augmentation to avoid undesirable effects caused by perturbation invariance, which is commonly used with GNNs and can create data distributions that appear as out-of-distribution (OOD) from an in-distribution (ID) graph. GoodD utilizes three hierarchical perspectives (Figure 1) to detect anomalies: feature view, structure view, and group view. The feature view includes node features (characteristics like bend, radius, eta, and phi). The structure view encompasses node degrees (directly connected edges) concatenated with the diagonal elements of the graph's random walk diffusion matrix. Lastly, the group view involves defining centroids of event groups after projecting them into an embedding space, providing the most general view of the analysis.<sup>2</sup>

---

<sup>1</sup> G. Li, C. Xiong, A. Thabet, B. Ghanem, Visual Computing Center, KAUST, 2020

<sup>2</sup> Liu et al., WSDM, Singapore, 2023

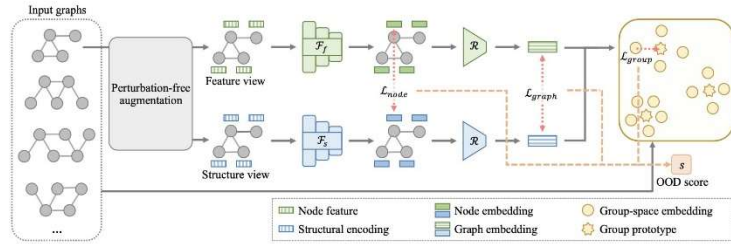


Figure 2: An overall illustration of the proposed method GOOD-D.

Figure 1

Currently the trigger that appears to have the best performance is an iteration of a GNN, with a yield rate of 40,976 events for a trigger rate of 77 KHz with a hit threshold of greater than or equal to 0 (Figure 2). Additionally the trigger reaches its peak efficiency at a hit threshold of greater than or equal to 30 hits and yields 82,202 events at a trigger rate of 77 KHz (Figure 3). The current trigger that has been proposed to the LHC yields about 16,000 events for a trigger rate of 77KHz at a hit threshold of greater than or equal to 0, which indicates that this trigger has outperformed the current benchmark.

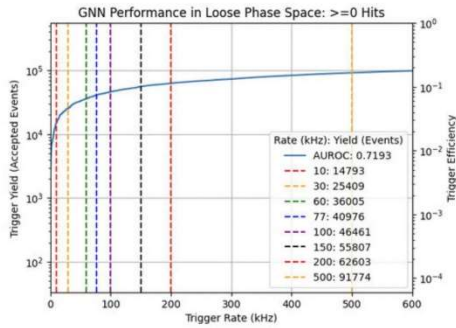


Figure 2

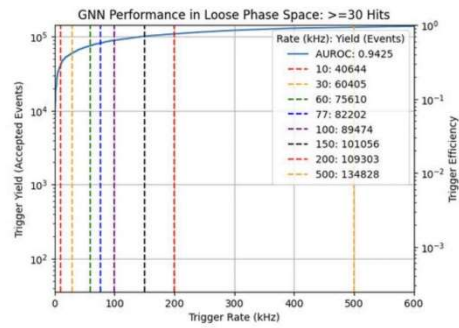


Figure 3

Acknowledgements: I would like to thank Dr. Miaoyuan Liu for her guidance and support throughout this project, while maintaining the importance of experimentation and room for growth. I would also like to thank Benjamin Simon for creating a supportive environment throughout the project, he is an effective teacher whose passion serves as an inspiration to those around him. This project was supported by NSF REU grant PHY-2244297.

# Macro Pixel Sub-Assembly (MaPSA) Testing for CMS Outer Tracker Upgrade

Emma Tintinger<sup>1,2</sup>, Mia Liu<sup>2</sup>, Jan-Frederik Schulte<sup>2</sup>

<sup>1</sup>University of Rochester, NY, <sup>2</sup>Purdue University, IN

CERN, the hub of the European Council for Nuclear Research, is home to the largest particle accelerator in the world, the Large Hadron Collider, or LHC [1]. In the LHC, powerful magnets along the collider steer the paths of two oppositely directed proton beams such that they collide with center of mass energy 14 TeV [13] at the sites of the four major detectors, LHCb, ATLAS, ALICE, and CMS [1]. The CMS (compact muon solenoid) experiment is an international collaboration that aims to use data from high energy collisions to uncover new insights about the inner workings of our universe [2].

Each section of the CMS detector serves a specific purpose [3]. The layers of silicon trackers around the beam pipe, composed of an inner and outer tracker [4], are used to reconstruct the paths of charged particles produced in particle collisions and subsequent interactions [3]. The curvature of these paths is a result of the magnetic field produced by the solenoid magnet in the detector's interior and can be used to extract key information about the corresponding particle's momentum and charge [3].

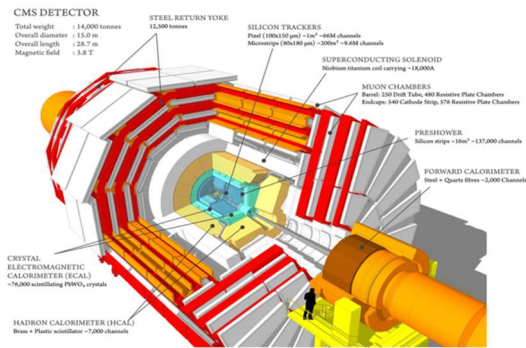


Figure 1 CMS detector components [3]

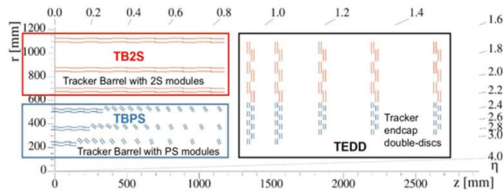


Figure 2 Planned upgrades to outer tracker [12]

The LHC is scheduled to undergo high luminosity upgrades in the coming years to increase its collision production [5]. Consequently, the CMS detector must undergo upgrades to efficiently handle this increase in radiation and data rates and improve granularity [4]. One key upgrade is the outer tracker upgrade, which includes the installation of Pixel-Strip (PS) modules [4]. These modules consist of a strip sensor and a MaPSA, which are both connected to a PS front-end hybrid readout chip [12]. These chips correlate hits from the strip and pixel sensors to determine a particle's transverse momentum for use in the L1 trigger logic [12].

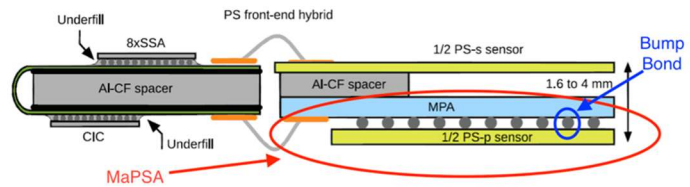


Figure 3 Diagram of PS module components [12]

Macro Pixel Sub-Assemblies, known as “MaPSAs”, consist of two main components [7]. The first is MPAs, or Macro Pixel ASICs (Application Specific Integrated Circuits) [8] [6].

There are 16 MPA chips per MaPSA module [8], which each read out data from 1888 sensor pixels that are 100 microns by 1.5 mm in size [9]. Silicon Macro Pixel sensors are then connected to the MPAs via bump bonding [8], a process in which sensor pixels are joined to ASIC pixels using metal solder balls [10]. Wire bond pads attached to the MPAs are used to connect the MaPSA to the readout chips for the full PS module [7]. Large scale MaPSA manufacturing is set to occur in 2024 and 2025, producing thousands of MaPSAs that will need to be tested prior to PS module assembly [7].



Figure 4 Close-up of the probe station in use [7]

MaPSA testing is done using a probe station [9]. The full setup consists of a circular chuck and vacuum ports that keep the MaPSA in place, a PC-controlled interface board with readout electronics, a probe card and attached probe needles, and an HV power supply establishing bias voltages [7][9]. The process begins by establishing electrical contact using probe needles [9]. We first align the small probe needles with the wire bond pads and then bring them into contact with the MaPSA [9]. The large needle makes contact with the sensors and is used to establish bias voltages whereas the small needles make contact with the wire bond pads and are used to send commands to the MPAs [9]. We run through a test suite to ensure the MaPSAs are functioning properly before eventually assigning a letter grade [9]. Grade A MaPSAs will go in the CMS detector, Grade B MaPSAs will be backups in case there are not enough Grade A MaPSAs, and Grade C MaPSAs will not go into the detector under any circumstances [9].

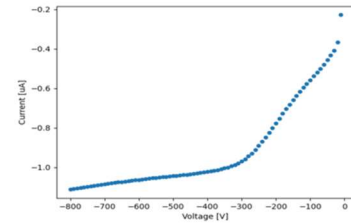


Figure 5 IV scan

Sensor functionality is assessed via an IV scan, which measures the total leakage current at varying bias voltages whereas ASIC functionality is assessed via a series of MPA tests [9][11]. These MPA tests assess memory function, built-in disabling measures, and pixel response to test pulses [9]. Finally, the connection between the sensor and ASICs is assessed via the bump bonding test, which uses noise levels to determine bump bond quality [9][11]. Non-dead pixels with noise levels well below average at a low bias voltage are considered to have an associated bad bump bond [9][11].

Larger-scale module testing is slated to begin in the fall, so the goal of my work this summer has been to ensure that Purdue will be well-prepared to run tests successfully and efficiently at that time. As part of this work, I researched the current testing code and documentation to get a deeper understanding of the purpose and function of each test. I then compiled what I learned into a testing guide for future students. Additionally, I helped troubleshoot existing equipment errors, added a capability for standalone remote plotting to the code, and investigated peculiarities in our observed data to identify the causes and test possible solutions.

I would first like to thank Prof. Liu for all her guidance and support this summer. Many thanks as well to Dr. Schulte for answering all my questions and always trying to help. I would also like to thank Dr. Dickinson and Dr. Berry for their thorough explanations. Finally, I would like to thank AJ Wildridge, Dr. Yao, and Ethan Colbert for their help as well as the entire particle physics group at Purdue for being so kind and welcoming. This project was funded by NSF REU grant PHY-2244297.

#### References:

1. <https://home.cern/science/accelerators/large-hadron-collider>
2. <https://home.cern/science/experiments/cms>
3. <https://cms.cern/detector>
4. [https://indico.desy.de/event/28202/contributions/105735/attachments/67494/83934/2021\\_07\\_27\\_ML\\_EPS.pdf](https://indico.desy.de/event/28202/contributions/105735/attachments/67494/83934/2021_07_27_ML_EPS.pdf)

5. <https://home.cern/science/accelerators/high-luminosity-lhc>
6. <https://www.techopedia.com/definition/2357/application-specific-integrated-circuit-asic>
7. Conversation with Jan-Frederik Schulte May 30<sup>th</sup>
8. [https://indico.cern.ch/event/916520/contributions/3853044/attachments/2035348/3407469/MPA\\_Test\\_proto.pdf](https://indico.cern.ch/event/916520/contributions/3853044/attachments/2035348/3407469/MPA_Test_proto.pdf)
9. Berry and Dickinson, MaPSA Round 2 Note (for internal distribution only), closest publicly available guide is <https://cds.cern.ch/record/2272264/files/CMS-TDR-014.pdf>
10. <https://indico.desy.de/event/12924/contributions/11019/attachments/7514/8851/bump-2016-03-MT.pdf>
11. Conversation with Jennet Dickinson June 8<sup>th</sup>
12. [https://indico.cern.ch/event/666427/contributions/2880250/attachments/1602428/2541055/Trento\\_CMS\\_OT-1.pdf](https://indico.cern.ch/event/666427/contributions/2880250/attachments/1602428/2541055/Trento_CMS_OT-1.pdf)
13. <https://cds.cern.ch/record/2809109/files/CERN-Brochure-2021-004-Eng.pdf>

# Rubidium-87 Magneto-Optical Trap

Bennett Hughes<sup>1,2</sup>, Rongjie Li<sup>2</sup>, Sambit Banerjee<sup>2</sup>, Chen-Lung Hung<sup>2</sup>

The Ohio State University<sup>1</sup>, Purdue University<sup>2</sup>

Since the first magneto-optical trap (MOT) was created to trap cold sodium atoms in 1987, they have been vital to advancements in cold atom physics and are the foundation of a variety of cutting-edge experiments. The process of forming a MOT, however, requires extremely precise lasers tuned to exact atomic transitions with high stability. I worked this summer to revive a laser system to cool and trap <sup>87</sup>Rb atoms, which will later be used to deterministically trap single atoms to couple to a nanophotonic waveguide.

A MOT traps atoms using laser radiation pressure and a magnetic field gradient to generate a confining force. Consider six counterpropagating laser beams shining on a cloud of neutral atoms. The laser's frequency is slightly red-detuned from an atomic resonance. As the atom propagates against the laser beam, the laser is Doppler shifted into resonance from the perspective of the atom. At resonance, absorption occurs, and the atom experiences a scattering force. The result is a viscous slowing effect. We then add a quadrupole magnetic field centered on the atom cloud. As an atom leaves the cloud, it experiences a magnetic field and has its atomic transition Zeeman shifted. This position dependent Zeeman shift allows our scattering force to confine the cloud, thus forming a MOT.

In order to address atomic resonances, the MOT lasers need to be able to resolve between individual hyperfine transitions. For <sup>87</sup>Rb, this means that the two 780nm lasers used in the setup (384 THz, separated by 6 GHz) need to be accurate within about 2 femtometers (<1 MHz), or about 2 ppb (parts per billion). To achieve this level of precision, everything about the lasers needs to be controlled to high accuracy.

This project required repairing two lasers and precisely locking their frequency. A new current controller had to be built from the PCB up, which can produce currents with noise levels within a few hundred nanoamps. Two external cavity diode lasers (ECDLs) were reassembled in the Littrow

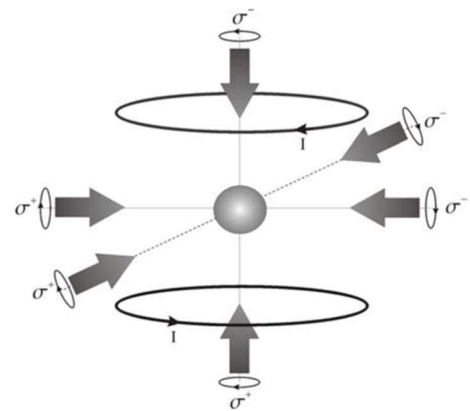


Figure 6: A 3D representation of magneto-optic trap (Credit: Krzysztof 2010)

configuration to achieve a narrow linewidth. The diffraction grating in the external cavity, which serves to precisely select output frequency, was then adjusted to optimize for the correct frequency and high power output. Both lasers were then locked at their correct frequencies, which was verified by looking at their beat note with a reference laser which was locked with spectroscopy.

At this point, the lasers have been prepared to form the MOT. The next step is couple them to a tapered amplifier to increase the power of the beams and begin the experiment, which has already been optimized based on previous testing. Once the MOT is formed, the setup may continue to be used to trap atoms in optical tweezers and eventually perform nanophotonic experiments.

I am incredibly grateful for the opportunity to do this work this summer. Thank you to Dr. Chen-Lung Hung for having me in his lab this summer, Sambit Banerjee for his exceptional guidance, and special thanks to Rongjie Li for helping me every step of the way. This work was supported by NSF REU grant PHY-2244297.



Figure 7: The current controller I assembled.

---

Krzysztof, K., V, C. L., Xuan, K. D., Małgorzata, G., Huy, B. N., & Jerzy, S. (2010). Magneto-optical Trap: Fundamentals and Realization. *CMST, Special Issue (2)*, 115–129.  
<https://doi.org/10.12921/cmst.2010.SI.02.115-129>

# Quantum sensing of paramagnetic ions with spin defects in hexagonal boron nitride

Troy Tsubota<sup>1,2</sup>, Sumukh Vaidya<sup>2</sup>, Xingyu Gao<sup>2</sup>, Peng Ju<sup>2</sup>, Tongcang Li<sup>2,3</sup>

<sup>1</sup>*Department of Physics, University of California at Berkeley, Berkeley, CA, 94720, USA*

<sup>2</sup>*Department of Physics and Astronomy, Purdue University, West Lafayette, IN, 47907, USA*

<sup>3</sup>*Department of Electrical and Computer Engineering, Purdue University, West Lafayette, IN, 47907, USA*

The negatively charged boron vacancy ( $V_B^-$ ) defect in hexagonal boron nitride (hBN), a two-dimensional van der Waals material, has proven to be a strong candidate for quantum sensing due to its wide band gap, high thermal conductivity, and excellent stability [1]. In particular, the  $V_B^-$  defect is capable of sensing paramagnetic ion concentrations which has important applications in studying physiological processes [2] and *in situ* measurement of the degradation of lithium-ion batteries [3].

The  $V_B^-$  defect is a spin-1 color center that can be optically initialized into the  $m_s=0$  state [1]. Under excitation by a 532 nm laser, these defects emit photons at around 830 nm. The different spin states emit at different rates, so the population of each state can be read out with a photon counter. Via the Zeeman effect, the energy levels split under a constant magnetic field. We can measure the splitting with optically detected magnetic resonance (ODMR), which finds the resonant microwave frequency between the energy levels from their different emission rates, to determine the strength of the magnetic field. Paramagnetic ions add magnetic noise to the system, decreasing ODMR contrast. The ion concentration can be measured from the magnitude of this change. The ion concentration can also be measured via a reduction in the  $T_1$  relaxation time, i.e., the time scale of  $V_B^-$  thermalization.

Recent work on paramagnetic ion sensing uses an hBN flake on a flat gold waveguide to sense  $Gd^{3+}$  ions [2]. However, the existing setup requires the laser light and  $V_B^-$  emission light to penetrate through the solution, which will not work for sensing environments that are opaque to 532 nm and 830 nm light. In addition,  $V_B^-$  defects suffer from low brightness, and precise readout can only occur with sufficiently high photon counts.

Therefore, in our work, we add cavities to the waveguide. The cavities allow for transmission through the bottom of the waveguide, thereby addressing the opacity problem. The cavities also enable stronger plasmonic enhancement. Tuning the resonant frequency of the cavity to align with the  $V_B^-$  emission frequency strongly increases brightness. However, there are drawbacks to this approach, such as larger resistance and heating. Most importantly, the magnetic field strength decreases above the cavity, making ODMR and relaxometry harder to perform.

To find an optimal design, we use COMSOL Multiphysics RF Module Frequency Domain Analysis simulations. We vary many parameters, such as the gold layer height, hBN layer height, cavity size, cavity shape, and cavity periodicity. We also test designs with gold nanopillars within the cavities—this increases plasmonic enhancement even further. We analyze the reflectance spectra and electric

field enhancement, seeking to match the resonant peaks at 532 nm and 830 nm. It is difficult to include additional analyses of magnetic field strength and ion concentration measurement within the same simulation. However, because the magnetic field strength decreases with the square of the period and ion concentration measurement decreases with  $d^6$ , where  $d$  is the implantation depth of the  $V_B^-$  defects, we minimize the period and implantation depth as much as possible. The resulting designs are on the nanometer scale, with optimal cavity diameters at  $\sim 100$  nm.

Then, we create GDS files in KLayout to proceed to nanofabrication. Fabricating an intricate design at this scale proves to be quite challenging; we test some simplified designs first. Electron-beam lithography fails because the cavity pattern washes away due to the small amounts of photoresist needed to create the cavities. Wet etching fails due to poor adhesion between the photoresist and gold. Additionally, the superacid needed to etch gold etches both horizontally and vertically, so precise nanoscale patterns are very difficult to create. Focused ion beam lithography shows promise [4] but precision on the sub-micron level remains a challenge.

Once we resolve nanofabrication issues, we aim to experimentally confirm the waveguide designs and verify existing ODMR and relaxometry results on  $Gd^{3+}$  ions. In the future, we look to use these designs to test broader applications, such as  $Mn^{2+}$  measurement in lithium-ion batteries. These designs (and variations of them) also hold promise for applications beyond ion sensing such as plasmonic enhancement of single carbon defects in hBN.

This work was supported by NSF REU grant PHY-2244297.

#### References:

- [1] S. Vaidya et al. Quantum sensing and imaging with spin defects in hexagonal boron nitride. *Advances in Physics: X*, **8**:1, 2206049 (2023).
- [2] X. Gao et al. Quantum sensing of paramagnetic spins in liquids with spin qubits in hexagonal boron nitride. arXiv preprint arXiv:2303.02326 (2023).
- [3] J. P. Allen et al. Quantifying Dissolved Transition Metals in Battery Electrolyte Solutions with NMR Paramagnetic Relaxation Enhancement. *J. Phys. Chem. C* **2023**, 127 (20), 9509–9521 (2023).
- [4] H. Cai et al. Spin Defects in hBN assisted by Metallic Nanotrenches for Quantum Sensing. *Nano Letters* **2023**, 23 (11), 4991–4996 (2023).

# Artificial Photosynthesis

<sup>1,2</sup>Betsy Woodward, <sup>1</sup>Yulia Pushkar, <sup>1</sup>Dileep Purayil, <sup>1</sup>Jully Patel, <sup>1</sup>Olga Maximova, <sup>1</sup>Gabriel Bury

<sup>1</sup> Purdue University, IN; <sup>2</sup> Grinnell College, IA

Artificial photosynthesis is a manner of taking the natural process of photosynthesis and artificially mimicking it to create fuel, from water and light. This is important because there is an ever-increasing demand for energy, while climate change and environmental destruction are growing in prevalence due to our overuse of fossil fuels. Currently, the main goal is to make the process of artificial photosynthesis more efficient so as to be an economically viable energy source. This requires the development of catalysts that are made from abundant materials and can function using visible light. Two useful methods of determining whether these potential catalysts would be effective are conductivity testing and Raman spectroscopy.

Conductivity testing is used to determine whether our samples absorb visible light. We can do so by seeing whether there's a difference between a sample's conductivity in the dark compared to when we shine visible light on it. Using our circuit set-up, we take the current reading from the multimeter, in addition to the known constant values of voltage and resistance, and use Ohm's law to solve for the resistance of the sample. Finally, using the resistance of the sample, as well as the known constant values of sample width and area, we can solve for the conductivity of the sample.

## Ohm's Law:

$$V = I (R + R_s)$$

$$R_s = (V/I) - R$$

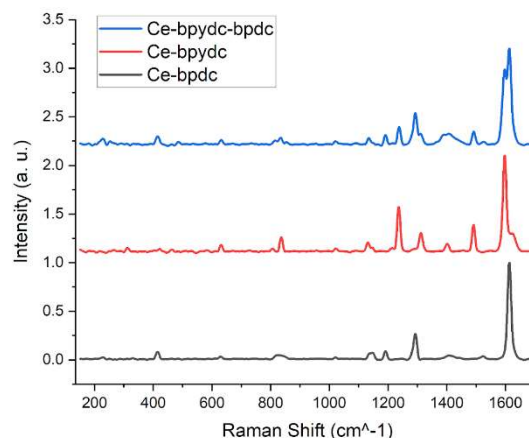
$$\sigma = t / (R_s * A)$$

where:

- $\sigma$  : sample conductivity
- $t$  : sample width
- $R_s$  : sample resistance
- $A$  : sample area

Raman spectroscopy involves shining a laser onto a sample and detecting the wavelengths of resulting light released from the sample. We then use the originpro software to edit the raw data to produce our final graphs. The peaks on these graphs are associated with a molecule's vibrations and can be analyzed in comparison to known characteristic vibrations from previous literature.

The graph to the right shows Raman spectroscopy results from the samples Ce-bpydc and Ce-bpdc. These are similar metal organic frameworks with only a few atoms difference, which is shown by how similar their Raman peaks are. We then took the combination of these two samples to form the new sample Ce-bpydc-bpdc, and took spectroscopy of all three. Using this graph, we can verify that all the peaks of the combined sample match up with a peak from at least one of the original samples.



I would like to thank Professor Yulia Pushkar for her mentorship this summer. I would also like to thank Dileep Purayil, Jully Patel, Olga Maximova, Gabriel Bury, and Vladimir for their instruction, assistance, and/or contributions to the research I participated in. This work was supported by NSF REU grant PHY-2244297.

### Sources

- Ezhov, R., Ravari, A. K., Palenik, M., Loomis, A., Meira, D. M., Savikhin, S., & Pushkar, Y. (2022). Photoexcitation of Fe<sub>3</sub>O nodes in MOF drives water oxidation at pH=1 when Ru catalyst is present. *ChemSusChem*, 16(5). <https://doi.org/10.1002/cssc.202202124>
- Jensen, S. (2018). Progress toward time-resolved x-ray spectroscopy of metalloproteins [Unpublished PhD dissertation]. Purdue University.
- Ravari, A. K. (2020). An investigation in the mechanism of [Ru(tpy)(bpy)(H<sub>2</sub>O)]<sup>2+</sup> and [Ru(bpy)<sub>2</sub>(bpyNO)]<sup>2+</sup> with the emphasize on the N-oxide: a redox active ligand [Unpublished PhD dissertation]. Purdue University.

# Acoustic Wave Propagation Through Fracture Networks

Mary J. Davenport<sup>1,2</sup>, Laura J. Pyrak-Nolte<sup>1</sup>, and David D. Nolte<sup>1</sup>

<sup>1</sup>Purdue University

<sup>2</sup>Gustavus Adolphus College

Many are interested in fractures in the subsurface, whether it is because they can be utilized for the flow of liquid or there are cases where the absence of fractures is required, such as hiding waste in the earth. Seismic waves are used to probe the subsurface for fractures; however, these waves have only been able to state the existence of a fracture. Can these waves decipher more about the fracture's properties? Using an asymmetric acrylic fractured sample in a laboratory setting, seismic waves were simulated using chattering dust and were analyzed to determine fracture spacing.

Using two 77 mm, two 12 mm, and three 19.4 mm wide acrylic blocks, an ideal sample with nonuniformly spaced 2 mm fractures was created. All – except for the outer fractures that were used for launching the chattering dust – contained a geometric plate insert analogous to the natural geometry of fractures in the subsurface. The nonuniform fracture spacing was investigated using piezoelectric contact transducers (1MHz), coupled to the sample with hot glue, that received the acoustic emissions from the chattering dust.

Using a Siamese triplet neural network, the waveforms collected were analyzed. Choosing two transducers directly across from each other to be compared, the waveforms examined were those that involved the chattering dust being launched in the fracture farthest from each transducer. The waves collected from one transducer should be different from those collected by the other due to the asymmetry of the sample. Yet, when fully saturated, the difference between codas for either launch fracture are negligible. In hopes that the neural net focused on the difference in codas in unsaturated cases rather than any inherent differences between the transducers, the two fully saturated cases were considered to be identical.

To confirm that the neural net was behaving as expected, a symmetric sample containing two 77 mm and five 12 mm wide acrylic blocks was used to create an ideal uniform fracture network with 2 mm spacing between blocks and geometric plates in the two inner most fractures. This sample was in hopes to prove that the neural network would ignore inherent differences between the transducers and focus merely on the codas. For the symmetric case, the codas should be identical, so the neural net should classify them as the

same. Results from this are still inconclusive, but this would prove that any classification made in the asymmetric sample is due to the difference in codas, illustrating how the waveforms of seismic waves through a fracture network carry information about the spacing of the fractures it travels through.

Assuming this condition, one hopes that the neural net will be capable of detecting the change in waveforms due to the nonuniform fracture spacing. Then, the seismic waves through fracture networks would be found to carry information about the spacing between fractures. With more research and data cleaning, the machine learning results can be improved, and more detailed information can be pulled from these acoustic propagations that can then be used in the field.

I would like to thank Professor Laura Pyrak-Nolte, Doctor David Nolte, and Alex Clark for the guidance they have provided me this summer and the incredible amount of knowledge that they have so kindly shared with me. This REU has been a growing experience thanks to their generous help through it all. This work was supported by NSF REU grant PHY-2244297.

# Integration and Assessment of Imaging Techniques in Applied Optics

James Szalkie<sup>1,2</sup>, David D. Nolte<sup>1</sup>

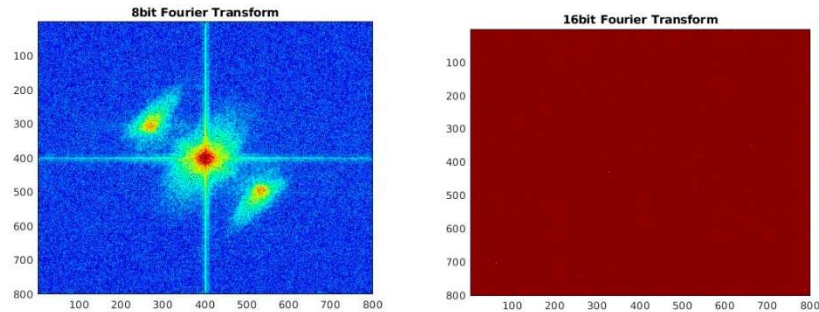
<sup>1</sup>Purdue University, IN; <sup>2</sup>Wabash College, IN

The study of light, imaging and holography is a widely integrated field, and crucial in many areas of study, ranging from biophysics and medicine, to geophysics and the study of seismology in a lab setting, both of which are approaches the group I was in this summer undertook. Due to unforeseen challenges in the lab that often arise in experimental and applied physics, my time was spent working on collecting data and analyzing the effectiveness of two imaging systems in the lab. My summer was dedicated to assembling the backbone, and testing the capabilities of two imaging systems in Professor Nolte's lab.

The initial phase of this summer's research tasked me to use a laser to detect sound waves in motion as they traversed a block of lucite. In the process of measuring the characteristics of the system, challenges such as unintended photoelastic and photoacoustic phenomenon demanded attention. What we found was that as the block of lucite underwent stress from the ultrasonic waves, local shifts in the density of the material allowed for the redirection of light to the photosensor, resulting in a clear and identifiable signal. This insight into the nature of the material will be helpful in determining aspects of the system once photography is integrated, and in determining the reliability and capabilities of the system in its final stages. While on this project we also devised a novel approach to timing entirely separate instruments to communicate and interact in a reliable and precise manner. Using a function generator as a trigger, and several 'daisy-chained' instruments, we created a working symphony of instruments that can be precisely adjusted for custom use. The integration and customization of this trigger will allow for future work on this project to be done in a reliable and accurate manner. Additional characterization and measurement of different aspects of this system, especially the pulsed laser on which it is all built around, will provide necessary data for future use.

The rest of my time this summer was devoted to Professor Nolte's novel approach to imaging biological samples under treatment. Using a coherent light source, a Fourier plate and a fresnel biprism, we are able to take scans of samples and record their movements. Because this is a fairly new and incredibly sensitive approach to optical imaging, this required thorough investigation and exploration. One aspect of the project required very simply to find the maximum capabilities of the system, pushing the depth and sensitivity of the camera and the software with which it operates. Additional investigation revealed further need for

shielding from environmental factors such as vibration and noise. However, the data collected this summer as well as assessments of the system made with Professor Nolte should lead to new approaches in this field in the near future.



Comparisons between the 8-bit and 16-bit capabilities of the camera reveal a limit to the effectiveness of data from this system. These are transforms from the Fourier plane the camera captures in, and the result are recreations of the image of the laser with sidebands. As seen here, the 16 bit setting oversaturated the camera, proving it to be ineffective for our uses.

In conclusion, the work and data collected this summer should serve to help to create more accurate and reliable imaging systems for this group in the future, and solidify the reliability of the conclusions that arise from this group's research. In the project centered around the imaging of sound in flight, the apparatus I constructed over my several weeks here will eventually be used for geophysics research to hopefully aid in carbon recapture, while the measurements and data collected on Professor Nolte's Fresnel biprism apparatus will help with future medical research, and refining its reliability.

**Acknowledgements:** I would like to thank Professor Nolte and his group for the opportunity I have been given this summer, and the guidance and advice he has given in the lab as unforeseen challenges arose. Thank you for teaching me how to keep a level head, even when everything is smoking. This work was supported by NSF REU grant PHY-2244297.

# Control of Superconducting Qubit Systems via RF Frequency Mixing

Nathan Henry<sup>1,2</sup>, Alex Ma<sup>2</sup>

<sup>1</sup>Purdue University, <sup>2</sup>Case Western Reserve University

Quantum Computing has become a major area of interest over the past few areas through its potential to greatly increase the speed of certain computations. Superconducting qubits are a particularly promising platform for computation as they can be manipulated using photon pulses and can be printed onto a chip. Thus, control and readout of such a quantum system is a crucial step towards realizing quantum computation. In particular, microwave pulses are sent to a resonator which is coupled with a transmon qubit whose state will be changed if the frequency of the microwaves matches the resonant frequency of the qubit.<sup>3</sup> These pulses can also be used to read the state of a qubit.

This project involves the implementation of one such method to control and read the qubit: using an IQ mixer to modulate a pulse so as to control not only the frequency sent to the qubit but also control the length of the pulse and thereby enable control and readout of the qubit.

For an IQ mixer, a base LO frequency is generated by an arbitrary waveform generator and then modulated using a mixer, which by using two (usually much lower frequency than the LO signal) RF signals, I and Q, at a  $\pi/2$  phase difference, result in a signal which, depending on the calibration of the mixer, ideally produces either the I frequency either added to or subtracted from the LO frequency.

Since the IQ mixer is not an ideal device, it does not produce only the desired sideband, but produces more generally both the addition and subtraction of the LO and I frequencies, as well as leaks some of the LO signal. This can be minimized through calibration, where the unwanted frequencies can be suppressed compared to the desired frequency by at least 60dB.

After implementing a calibration script, this process can be done automatically and the results appear promising, with the unwanted signals usually suppressed by over 60dB. By also implementing a software switch, this calibration can be done entirely hands-free, which is important as the optimal configuration can change with the ambient temperature, the frequency of the LO, and the frequency of I and Q.

I would like to thank Pf. Ma and Botao Du for their help and support while I worked in Pf. Ma's lab. I would also like to thank Purdue's physics department for giving me this opportunity to learn and experiment. This work was supported by NSF REU grant PHY-2244297.

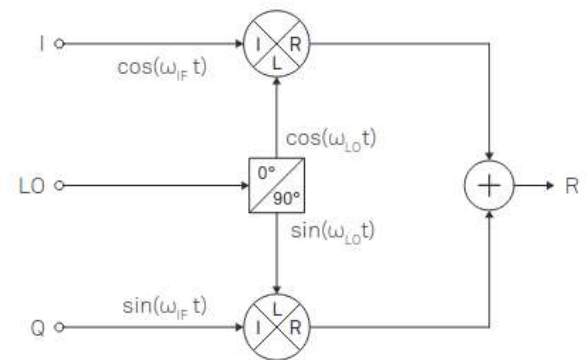


Figure 8: Schematic of an IQ mixer

3 Zurich Instruments. Frequency Up-Conversion of Arbitrary Waveform Generators. Zurich Instruments, August 2018.

# Designing and Implementing PID Controller to aid in Investigating the Photoassociation of Rb-87 Bose-Einstein Condensates

Julia White<sup>1,2</sup>, Felicia Martinez<sup>2</sup>, Chuan-Hsun Li<sup>2</sup>, Yong P. Chen<sup>2,3,4</sup>

<sup>1</sup> *Department of Physics and Astronomy, Bates College, Lewiston, ME*

<sup>2</sup> *Department of Physics and Astronomy, Purdue University, West Lafayette, IN*

<sup>3</sup> *School of Electrical and Computer Engineering, Purdue University, West Lafayette, IN*

<sup>4</sup> *Purdue Quantum Center, Purdue University, West Lafayette, IN*

Bose-Einstein Condensate (BEC) is a state of matter that is formed when atoms are cooled very close to absolute zero. We would like to use them as a highly controllable quantum system for the study of quantum chemistry.

Photoassociation occurs when two freely scattering atoms are excited by a resonant laser beam and form into a single molecule in their excited state. The Purdue AMO-BEC lab would like to study photoassociation (PA) in Rb-87 BECs that are prepared in a quantum superposition state. To do so, a pair of counter-propagating Raman lasers are used to couple the internal spin states of an atom. This also can be done using Radio Frequency (RF) dressing wherein the atom's internal energy levels are coupled by an RF electromagnetic field. Photoassociation spectroscopy is then performed and the PA rate can be extracted.

The power fluctuations of the laser beam that is used to photoassociate the atoms will create an uncertainty in the measured rate of the photoassociation process. The beam is generated from a Ti Sapphire laser with approximately 50 MHz steps which is tuned close to our desired PA resonance. The beam is then double passed through an acoustic optical modulator to sweep the frequency in smaller steps of about 5 MHz. When this frequency is changed, the power output also changes because the efficiency of the acoustic optical modulator varies with different applied frequencies. This is corrected by the voltage-controlled attenuator but this requires careful calibration for each desired laser power to be used in the experiment. One way to reduce the need for a power calibration for each experiment as well as to reduce the overall fluctuation is to implement a proportional-integral-derivative or PID control circuit which stabilizes the laser power.

To provide feedback to the circuit, a sample of the beam is taken into a photodiode which converts the incident power into voltage. This allows the circuit to compare this voltage to a chosen set voltage and the controlled output then generates a correction to be applied to the voltage-controlled attenuator. Once this controller was built and implemented, it was tested. The power

fluctuation range to the optical fiber over five seconds was found with and without the PID controller being used. The width of this range was then divided by the typical power to the fiber at that set voltage, allowing the power fluctuation as a percentage of the typical power to be found. This was about 1.73% on average when controlled and approximately 4.18% when uncontrolled. Using the controller also meant that by changing the set voltage, the power to the fiber could easily be adjusted using a recorded proportional scale. This controller was shown to maintain a consistent beam power while scanning the frequency with the acoustic optical modulator, meaning that more frequencies can be easily used. This will help increase the consistency of our photoassociation measurements.

I would like to thank Professor Yong P. Chen, Dr Chuan-Hsun Li, and Felicia Martinez for their insight and guidance in this project. This work was supported by NSF REU grant PHY-2244297.

# Automation of Time Series Giga-hertz Data Streams from Circuits

*Lauren Bell, Jhinkyu Choi, Arnab Banerjee*  
Purdue University, IN

As most strongly-correlated electronic materials are cooled to low temperatures, the spins of electrons become arranged in an organized pattern without further fluctuation. In the presence of geometric frustration, on the other hand, the electrons can form Quantum spin liquids (QSLs) which never become magnetically ordered even when cooled to absolute zero.<sup>[1]</sup> These materials give rise to exotic quantum effects, such as new quantum quasiparticles, that have the potential to protect quantum information from decoherence.

The search for such quantum spin liquids is a strong research endeavor in condensed matter physics and material science. One way to achieve that is to probe the noise generated by the materials due to quantum fluctuations when transduced using Pt-electrodes.<sup>[2]</sup> However, such experiments are difficult due to the confounding effects of ambient RF noise, necessitating the use of ultrasensitive and low noise electronics combined with the correct filters to eliminate any undesired noise sources. This project makes an effort to collect large giga-hertz data streams of noise from cryo-circuits and help evaluate the electronics that enable this acquisition.

Specifically, we are using the Tektronix MSO46, a mixed signal oscilloscope capable of measuring up to 6.25 billion samples per second as well as spectrum analysis to 6 GHz. Automating this instrument included balancing three primary variables: the sample rate, the number of samples making up each waveform, and the number of waveforms generated each second. These variables must be maximized as much as the oscilloscope allowed while ensuring it was still physically possible to collect all generated data. Several obstacles were encountered and investigated, including the methods used to perform multiple operations in Python simultaneously, the rates at which data was transferred between the oscilloscope and PC, the constraints of various acquisition modes, timing the data collection batches, and saving significant amounts (Giga-bytes) of data continuously. Further work on this instrument will include potential updates to the firmware, which enables faster data transfer rates, testing the efficiency of mixing Python with C++ to accelerate specific program functions, and performing operations on a cluster. The procurement of a dedicated spectrum or network analyzer is also discussed as a part of the project.

A Lakeshore Model 372, an AC resistance bridge and temperature controller, is used in experiments and underwent the automation process. This instrument's program followed a

similar approach to writing the oscilloscope code and therefore took less time to complete. In comparison to the MSO46, this instrument does not need to collect as much data, and thus the automation did not encounter as many obstacles.

The continuing work will involve the integration of the Python code with Oxford ProteoxMX, a dilution refrigerator, to control the temperature and magnetic field and read out those values and any generated data. Alongside the automation of all instruments, different cryo-attenuators and cryo-amplifiers are being used to reduce the undesired noise present in measurements, and further configuration of the instruments' settings to enhance acquisitions can be done.

To ensure consistency of the measurements, all instruments used during the experiments are automated via Python. Python will also send Standard Commands for Programmable Instruments (SCPI) and specific package commands to configure each instrument with the desired settings. Automation entails beginning data acquisition of all instruments simultaneously when the user specifies, then collecting the data continuously while simultaneously saving all data and displaying it in real-time to the user. The GUI is being designed to obtain and store all the data parallelly and time-stamped. The noise time-series data obtained thus is being analyzed using Fast Fourier transform to obtain the power spectrum and its frequency dependence to seek the proper scaling laws which could carry the telltale signatures of the quantum fluctuations as a function of temperature and magnetic field – which is the ultimate goal of the work.

### **Acknowledgments**

Thank you to Professor Arnab Banerjee for his continued mentorship, instruction, and support throughout this project. Thank you to Jhinkyu Choi, Luis Henrique Vilela Leão, and Gabriel Goodwin for their assistance. This work was supported by NSF REU grant PHY-2244297.

### **References**

- [1] Broholm, C., Cava, R. J., Kivelson, S., Nocera, D. G., Norman, M. R., & Senthil, T. (2020). Quantum spin liquids. *Science*, 367(6475). <https://doi.org/10.1126/science.aay0668>
- [2] Idzuchi, H., Kimata, M., Okamoto, S., Laurell, P., Mohanta, N., Cothrine, M., Nagler, S.E., Mandrus, D., Banerjee, A., Chen, Y.P. et al Spin sensitive transport in a spin liquid material: revealing a robustness of spin anisotropy. *arXiv:2204.03158*

# Resonant Tunneling due to Impurities in the $\nu=1$ Quantum Hall State

*Daniel Hoover<sup>1,2</sup>, Jukka Vayrynen<sup>1</sup>*

*<sup>1</sup>Purdue University, <sup>1,2</sup>Lafayette College, PA*

The integer quantum Hall effect refers to the quantized version of the Hall effect observed in two-dimensional electron systems under strong magnetic fields, where electrons form one-dimensional edge states at low energies with integer quantum numbers. By constructing a uniquely shaped system, these edge states can be made to interfere with one another. In particular, a system consisting of a channel with two quantum point contacts (QPCs) can be made into an Aharonov-Bohm interferometer. This type of interferometry is possible not only in the integer quantum hall effect, but also in the fractional quantum hall effect, where it proves to be a powerful tool for probing anionic braiding.

In a broader context, this research contributes to the understanding of interferometry in fractional quantum Hall states and illuminates the effects of impurity levels on electronic transport properties. Potential applications encompass the design of novel nanoscale devices exploiting quantum interference effects and the development of quantum information processing technologies based on anionic braiding in fractional quantum Hall systems.

This project numerically explores quantum point contacts within systems under a strong magnetic field, such that the edge states due to the quantum Hall effect follow the edges of the QPC. This scenario was simplified as a tight-binding system and simulated using the Kwant software package.<sup>1</sup>

In particular, this project aims to focus on the impact of an impurity level within one of the quantum point contacts in an Aharonov-Bohm interferometer, where such an impurity acts as a quantum dot with multiple energy levels. While ordinarily a quantum point contact has a transmission floor that depends on its physical properties, such an impurity has the potential to induce resonant tunneling behavior, where an electron with an energy that matches one of the energy levels of the quantum dot is able to traverse the quantum point contact, even when their energy falls below the conventional transmission threshold. This has potentially unexpected effects on experiments that feature quantum point contacts.

An Aharonov-Bohm interferometer with two quantum point contacts was numerically constructed in Kwant. Edge states were observed, along with the corresponding band structure. Within this system, a single electron can traverse an arbitrarily high number of loops within the interferometer before escaping it, such that the electron can take an infinite number of pathways through the system. When calculating transmission for a range of energies, interference patterns were observed.

It remains to ascertain how to simulate a quantum dot within Kwant. There are several possibilities, but one in particular presents itself. One feature of the interferometer setup is that while the second quantum point contact increases the transmission floor overall, an electron that constructively interferes within the interferometer is likely to transmit even below the conventional transmission floor. This opens up the possibility to simulate an impurity within a quantum point contact by creating an interferometer in miniature. However, it remains to be seen whether the scale of this miniature interferometer-within-interferometer will present numerical issues within Kwant.

I would like to thank Prof. Vayrynen and his team for guiding this project at every step. This work was supported by NSF REU grant PHY-2244297.

References:

[1] C. W. Groth, M. Wimmer, A. R. Akhmerov, X. Waintal, Kwant: a software package for quantum transport, *New J. Phys.* 16, 063065 (2014).